BBA 75693

CIRCULAR DICHROISM OF BIOLOGICAL MEMBRANES

I. MITOCHONDRIA AND RED BLOOD CELL GHOSTS

D. W. URRY, L. MASOTTI AND J. R. KRIVACIC

Division of Molecular Biophysics, Laboratory of Molecular Biology, University of Alabama Medical Center, Birmingham, Ala. 35233 (U.S.A.)

(Received February 22nd, 1971)

SUMMARY

Improved circular dichroism curves are reported for mitochondria and red blood cell ghosts. The red shift and low amplitudes of the suspension spectra are shown to be due to distortions arising from the particulate nature of the samples. Previously proposed details of membrane structure based on the "red shift" are not supported by the corrected spectra.

Sources of the distortion may be classified as concentration obscuring and differential scatter effects. The concentration obscuring effects are due to the absorption flattening of Duysens and dispersion distortions or light scattering. As the membranes are optically active particles, they differentially scatter left and right circularly polarized light. Several approaches are outlined for correcting the membrane spectra. Particularly emphasized is a relatively simple and direct method for approximating an improved ellipticity at 224 nm.

The improved spectra are characteristic of α-helical protein and polypeptide systems in which about 50 % of the protein is in the α-helical conformation. Extrapolating from this correspondence is somewhat hazardous but would likely be more meaningful for mitochondrial and red blood cell membranes than for other membranes with lower ellipticities.

INTRODUCTION

In the past several years numerous papers have appeared which reported the optical rotation (optical rotatory dispersion and circular dichroism) spectra of biological membranes[1–9]. The spectra resembled those characteristic of α-helical proteins and polypeptides, but they were red shifted and of low amplitude. While many of these reports contained discussions and analyses of the possible significance of the results, others boldly extrapolated to specific interpretations leading to proposals of detailed membrane structure. More recently it was proposed that the red shift and low amplitude were artifacts due to the particulate nature of the systems[10], and experimental results were reported which supported this contention[11]. Subsequently, independent laboratories have confirmed the basic assertion and nature of the distort-

ed spectra[22]. It is necessary to state that the optical rotation data do not provide a basis for the bold extrapolations to details of membrane structure.

Two considerations were shown to be important in distorting suspension optical rotation spectra; these are wavelength dependent concentration obscuring effects[13,14] and differential scatter of left and right circularly polarized light by the optically active particle[15]. The concentration obscuring effects are due to absorption flattening as described by DUYSENS[16] for absorption spectroscopy and due to light scattering, *i.e.* dispersion distortion effects. The absorption flattening effect may be described as a particle casting a shadow obscuring the chromophores in the light path behind the particle. The shadow becomes darker as the absorption of the particle increases. This leads to a flattening of the absorption maxima. The obscuring of chromophores arising from light scattering is simply due to the probability that the light scattered by the particle would have been absorbed had the sample been molecularly dispersed. The obscured concentration in the latter case is proportional to the product of the probabilities of scatter and absorption[13]. Both concentration obscuring effects are wavelength dependent. In absorption flattening, as noted above, when the absorption of the chromophore increases, the shadow cast by the particle becomes darker and fewer chromophores are reached by the beam. In the light scattering effect, the scattered light is dependent on the square of the difference in solvent and particle refractive indices. Since refractive index is anomalous in absorption regions, the chromophores obscured by this process can change dramatically with wavelength. Also the differential scatter effect in circular dichroism has the appearance of the Cotton effect of an optical rotatory dispersion curve, thereby further distorting the circular dichroism spectrum in a highly wavelength dependent manner.

In attempting to improve the optical rotation data on particulate systems we have taken a semi-empirical point of view. We have derived expressions for the several effects noted above and then have carefully considered model systems in order to determine the most useful forms of the derived expression. Thus, the form of the expression for calculating distorted spectra or for correcting distorted spectra is decided upon by application to model systems. In this connection we found poly-L-glutamic acid to be a most useful model system. Accordingly, under specified experimental conditions of concentration, average particle size, and path length for the model system studies, we determined whether the absorption flattening and light scattering concentration obscuring effects should be treated in a product or an additive fashion[14]. The criterion was, of course, the best fit of the distorted curve.

In the process of obtaining the required parameters it was realized that one should use the same phototube for both the circular dichroism and absorption measurements. This allows one to know exactly the absorption exhibited by the sample during the optical rotation measurements. Accordingly, the instrument was modified in order to obtain absorption data from the dynode voltage of the circular dichroism photomultiplier. This process has been broadly outlined previously[14] and a detailed description will be forthcoming[17].

There are two fundamental differences between absorption and circular dichroism data on particulate systems. One is the complicating presence of differential scatter in the circular dichroism data[15]. The second is that the absorption flattening and light scattering effects work in concert in the circular dichroism to decrease ellipticity, whereas in absorption, the flattening, of course, decreases absorption but

the light scattering leads to an increase in measured absorption such that the two effects are opposed. This leads to a cross-over in the absorption of the molecular dispersed and particulate samples. The cross-over point occurs at the wavelength where the decrease due to concentration obscuring is exactly matched by the increase in absorption due to light scattering. When the cross-over occurs at an adequate wavelength, for example 10 nm from the absorption maximum, an iterative procedure can be used to calculate the absorption due to scatter, A_S, and the true absorption of the suspension. Knowledge of the true absorption curve for the suspension and the absorption for the molecularly dispersed sample allows calculation of the flattening quotient, Q_A. This approach was used in calculating the distorted spectrum of particulate poly-L-glutamic acid[14].

For many systems of interest the absorption is quite low, near 225 nm, such that the absorption flattening can be neglected in the first approximation. Furthermore, at this wavelength, the differential scatter is negligible for systems with α-helix-like optical rotation spectra. Accordingly a reasonable approximation of the correct ellipticity can be achieved by obtaining an approximate value for the absorption due to scatter at this wavelength. The approximation of a correct value near 225 nm can be used to identify a pseudo reference state, *i.e.* a molecularly dispersed state obtained by dissolution of the membrane system of interest. The pseudo reference state can then be used to generate improved circular dichroism curves for the particulate system[18].

Another approach to calculating an improved spectrum is to construct an average index of refraction of the particle. With the particle refractive index the absorption due to light scattering, A_S, in the wavelength regions where true absorption is negligible can be fitted using either the Rayleigh–Gans or Mie equation[14,19]. With the fitted equation and the wavelength dependence of the particle refractive index it is possible to calculate A_S throughout the absorption region. These several approaches are tested on the model poly-L-glutamic acid system and will be demonstrated in this paper and the following papers in the series on biological membranes.

In the present work we treat mitochondria and red blood cell membranes together, since these systems have the highest ellipticities. The second paper in the series deals with plasma membranes and sarcotubular vesicles[20]. The latter membranes, and particularly the sarcotubular vesicles, represent a transition to membranes with lower ellipticities and higher absorptions as exemplified by axonal membranes which are to be treated in a subsequent paper. From these results one begins to recognize a correspondence between absorption and circular dichroism spectra on the one hand and functionality of the membrane on the other.

METHODS

Beef heart mitochondria were isolated according to the method of CRANE *et al.*[21] with minor modification. The ground meat was washed using 950 ml of 0.9 % KCl, 0.01 M K_2HPO_4 medium for every 700 g of meat; it was then squeezed through a double layer of cheese cloth. The isolated mitochondria were washed twice in buffer and suspended in a volume of buffer giving a protein concentration of approx. 25 mg/ml.

Red blood cell ghosts were prepared according to DODGE *et al.*[22]. The erythro-

cytes from human venous blood, previously defibrinated, were washed and hemolyzed at a constant pH of 7.4 and a temperature of 4°. Repeated hemolyses were carried out using progressively more hypotonic buffer phosphate solutions until a final solution of 20 imosM was reached. The ghosts, examined under a light microscope, showed a pattern of regular, spherical vesicles.

In order to achieve smaller particle size sonication was used. The membranes were finally dissolved with detergents and solvents, and sonication was carried out with an M.S.E. Ultrasonic Disintegrator (60 W) used at an intensity output of 1.1 A. Three ml of suspension were put in a test tube 1 inch in diameter and 2 inches deep, purchased from Heat Systems Co., and were kept in ice and sonicated in alternating steps of 30 sec each.

Trifluoroethanol, purchased from Halocarbon Products Corp., was distilled according to KRIVACIC AND URRY[23]. Sodium dodecyl sulfate was purchased from Eastman Organic Chemicals and recrystallized twice from 95 % ethanol. The samples were stirred for 1.5 h at room temperature in 0.2 % sodium dodecyl sulfate. When trifluoroethanol and sodium dodecyl sulfate were used at the same time, the ratio of detergent-treated sample to trifluoroethanol was 1:4.

The circular dichroism of the samples was measured on a Cary Model 60 spectropolarimeter with Model 6001 attachment for circular dichroism and an accessory for simultaneous measurement of absorption[17]. For mitochondria, a 0.1-mm path length cell was used when the sample was in phosphate buffer, and a 0.5-mm path length cell was used when the suspension was diluted 5 times with trifluoroethanol. For the red blood cell ghosts, 0.2-mm and 1.0-mm path length cells were used. The protein concentrations determined, by the biuret method, were in the range of 1.8–2.2 mg/ml for all scans. Electron micrographs were obtained on the membrane preparations to determine purity of preparation and to assess homogeneity of particle size. The size of the sonicated particles were primarily in the 0.1–0.2-μm range. In the sonication series each sample after each serial sonication was re-run in the same spectrophotometer cell.

RESULTS AND DISCUSSION

Mitochondrial membranes

The circular dichroism data on mitochondria as a function of sonication and on addition of trifluoroethanol are given in Fig. 1. As the average particle size is decreased with sonication there is a large enhancement of ellipticity and concomitantly there is a return of the long wavelength extremum from its red shifted position to a position more characteristic of molecular dispersed α-helical systems. This effect was observed with poly-L-glutamic acid suspensions[11,14] and also previously reported for mitochondria[11]. Due to our absorption accessory we can now report the simultaneously recorded absorption spectra (see Fig. 2). The most striking effect, in absorption, of sonication is the many-fold increase in absorption at low wavelength range. This is due to decreased absorption flattening corresponding to decreased particle size. The absorption spectrum of the sample made molecularly dispersed by addition of trifluoroethanol can be compared to Curve a to get a gross idea of the increase in absorption due to light scattering.

It should be noted that light scattering is a complicated function of particle

size, wavelength and angle of measurement with respect to the transmitted beam. When the particles are large, the scattered light is primarily in the forward direction and the intensity of scattered light does not necessarily increase with decreasing wavelength[24]. Accordingly part of our purpose in sonicating is to bring the particle size into a range which is closer to that of our model studies. This allows that the considerations shown to be adequate under conditions of our model studies would then be more applicable to the biological membrane studies. Our interest then centres on correcting Curve a of Fig. 1.

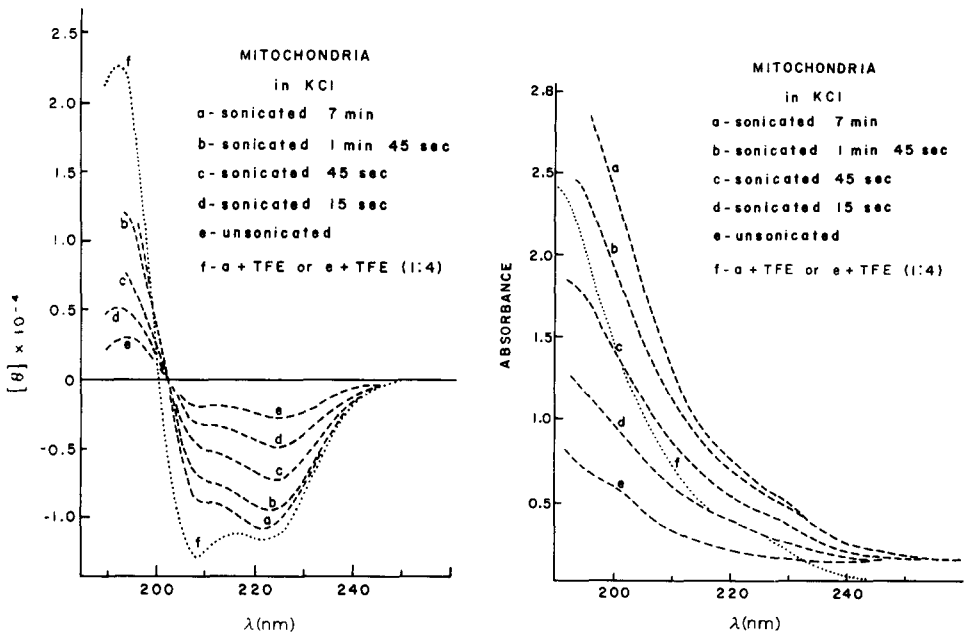

Fig. 1. Circular dichroism curves of mitochondria. Progressive sonication results in progressive increases in magnitude of ellipticity. The concentration of protein was 1.88 mg/ml and the path length 0.213 mm. Addition of four parts of trifluoroethanol (TFE) to Sample a or e giving a molecularly dispersed solution resulted in a further increase in ellipticity. Also note the progressive red shift of the long wavelength extremum as one approaches the intact mitochondria, *i.e.* as the particle size increases (see Fig. 2).

Fig. 2. Absorption curves obtained simultaneously with the circular dichroism curves in Fig. 1. At low wavelengths sonication results in increased absorption due to decreases in particle size leading to less absorption flattening. This evidence for increase in particle size in going from Curve a to Curve e should be correlated with the progressive red shift of the long wavelength circular dichroism extremum in Fig. 1.

Initial approximation of $[\theta]_{corr}^{224}$:

At wavelengths near those where optical rotatory dispersion curves are zero, *e.g.* 224 and 192 nm, the differential scatter effect is negligible. When this is true the correct ellipticity, $[\theta]_{corr}$, can be approximated by the expression[14,15]

$$[\theta]_{corr} \simeq \frac{[\theta]_{susp}}{Q_A - A_S} \tag{1}$$

where A_S is that part of the absorption measured by the photomultiplier which is due

to light scattering, and Q_A is the flattening quotient of DUYSENS[16] now defined as

$$Q_A = \frac{A'_{susp}}{A_{soln}} \tag{2}$$

where the measured absorption of the suspension, A_{susp}, is

$$A_{susp} = A'_{susp} + A_S \tag{3}$$

Furthermore, near 224 nm the absorption by the molecules that comprise the particle is low (see Curve f in Fig. 2). This means that Q_A^{224} is only slightly different from 1 and may be taken as such in the first approximation. Hyper- and hypochromism effects arising from interactions of chromophores within the structured membrane can be substantial at 192 nm such that before one can make extrapolations from the molecularly dispersed, dissolved membrane spectrum, a basis for doing so is required. Fortunately hyper- and hypochromism are not so significant at 224 nm. Thus, for a first approximation we can write

$$[\theta]_{Cl}^{224} = \frac{[\theta]_{susp}^{224}}{1 - A_S^{224}} \tag{4}$$

The absorptions for Curves a and f of Fig. 2 are 0.69 and 0.36, respectively, and the ellipticity for Curve a of Fig. 1 is $-1.07 \cdot 10^4$. From Eqns. 3 and 4 we have that $A_S^{224} \simeq 0.33$, and that $[\theta]_{Cl}^{224} = -1.6 \cdot 10^4$. This approach to approximating $[\theta]^{224}$ is very simple and as will be shown below is a very good approximation to the value obtained after more extensive calculation. It is particularly satisfying that the ellipticity at 224 nm is essentially the same as at 222 nm, which is the wavelength extremum commonly found for α-helical structures and, therefore, the wavelength from which approximations of helical content are often calculated, however, gross such calculations may be. Such calculations have a higher probability of being meaningful for mitochondrial and red blood cell membranes than for the plasma membranes and particularly the sarcotubular vesicles to be treated in the next paper in the series. Eqn. 4 and the considerations behind it provide the most direct and simple route for obtaining a useful improved ellipticity value for particulate systems.

Calculation of complete spectrum

Complete spectral calculations are much more involved requiring calculations of Q_A and A_S at all wavelengths as well as the change in ellipticity due to differential scatter of left and right circularly polarized light. The contribution due to differential scatter is designated[15]

$$\Delta[\theta]_{DS} = A_{SL} - A_{SR} \tag{5}$$

$$A_{SL} = -0.434 \ln \left[1 - \frac{K_D}{\lambda^v} \left(\frac{n_{PL}^2 - n_S^2}{n_{PL}^2 + 2n_S^2} \right)^2 \right] \tag{6}$$

$$A_{SR} = -0.434 \ln \left[1 - \frac{K_D}{\lambda^v} \left(\frac{n_{PL}^2 - n_S^2}{n_{PR}^2 + 2n_S^2} \right)^2 \right] \tag{7}$$

$$n_{PL} = n_P + \frac{(n_L - n_R)_P}{2} \tag{8}$$

$$n_{PR} = n_P - \frac{(n_L - n_R)_P}{2} \tag{9}$$

$$(n_L - n_R) = \frac{[m]\lambda\rho_P}{18\,mw} \tag{10}$$

n_P and n_S are the index of refraction of the particle and solvent respectively; K_D is the dispersion distortion coefficient; $[m]$ and ρ_P are the mean residue rotation and density of the particle; λ is the wavelength in centimeters, and mw is the mean residue molecular weight. K_D and the exponent v of λ^v are obtained by fitting the absorption due to scatter in a wavelength region where there is little true absorption. For mitochondria the wavelength region chosen was 300–240 nm, and the general equation for A_S was used, *i.e.*

$$A_S = -0.434 \ln\left[1 - \frac{K_D}{\lambda^V}\left(\frac{n_P^2 - n_S^2}{n_P^2 + 2n_S^2}\right)^2\right] \tag{11}$$

However, before this can be done the index of refraction of the solvent and particle are required as a function of wavelength. n_S was directly measured for the solvent system using the variable angle single reflectance method[23]. n_P was determined in a manner analogous to that used for the poly-L-glutamic acid particles[15,25] and poly-L-alanine films[19]. The density of the mitochondria was measured to be 1.14 by CsCl density gradient centrifugations. The composition of beef heart mitochondria was taken from LEHNINGER[26] and the size of the particle was taken as 0.1 μm (ref. 27). Using index of refraction data on cyclohexane and acetic acid, *etc.*, in connection with densities and concentrations of CH_2 moieties, peptides, esters and carboxylic acids, an adequate n_P could be approximated. The values of n_P and n_S are given in Table I. Using Eqn. 11 and the refractive indices in Table I, the values of A_S can be calculated.

TABLE I

REFRACTIVE INDICES OF MITOCHONDRIAL PARTICLES, n_P, AND OF THE SOLVENT SYSTEM, n_S, DIRECTLY MEASURED BY THE VARIABLE ANGLE SINGLE REFLECTANCE METHOD[23]

n_P is calculated using the dispersive parts of the partial refractive indices of dimethylformamide, cyclohexane and acetic acid.

λ (nm)	n_P	n_S
240	1.58612	1.38342
236	1.59716	1.38578
232	1.61478	1.3883
228	1.63048	1.39098
224	1.64002	1.39385
220	1.64653	1.39693
216	1.65768	1.40023
212	1.67655	1.40377
208	1.69953	1.4076
204	1.71979	1.41173
200	1.72664	1.4162
196	1.70631	1.42106
192	1.65164	1.42635
188	1.57125	1.43213

TABLE II

VALUES OF Q_A, THE FLATTENING QUOTIENT; A_S, ABSORPTION DUE TO SCATTER; A_{SL} AND A_{SR}, THE ABSORBANCES DUE TO DIFFERENTIAL SCATTER; AND THE CORRECTED ELLIPTICITIES FOR MITOCHONDRIA

$\Delta[\theta]_{DS}$ is the correction for differential scatter.

λ (nm)	Q_A	A_S	$Q_A - A_S$	A_{SL}	A_{SR}	$\frac{[\theta]_{susp}}{Q_A - A_S} - \Delta[\theta]_{DS}$
240	0.9865	0.170378	0.8161	0.170286	0.170469	—0.1920
238	0.9850	0.182122	0.8029	0.182012	0.182232	—0.2955
236	0.9852	0.196264	0.7889	0.196134	0.196395	—0.4084
234	0.9856	0.212864	0.7727	0.212755	0.213013	—0.5742
232	0.9835	0.231135	0.7524	0.230986	0.231283	—0.7411
230	0.9810	0.249329	0.7316	0.249182	0.249476	—0.9489
228	0.9771	0.265087	0.7120	0.264961	0.265212	—1.2261
226	0.9723	0.276581	0.6957	0.276500	0.276662	—1.3636
224	0.9687	0.283612	0.6851	0.283593	0.283630	—1.490
222	0.9665	0.288048	0.6785	0.288087	0.288009	—1.5833
220	0.9631	0.293016	0.6701	0.293103	0.262930	—1.5396
218	0.9601	0.301871	0.6582	0.302005	0.301738	—1.5302
216	0.9557	0.317110	0.6386	0.317295	0.316926	—1.5459
214	0.9515	0.340214	0.6113	0.340451	0.339977	—1.5744
212	0.9469	0.371432	0.5755	0.371757	0.371107	—1.6868
210	0.9381	0.410235	0.5279	0.410689	0.409781	—1.8480
208	0.9278	0.454916	0.4729	0.455662	0.454172	—1.8925
206	0.9173	0.501914	0.4154	0.503071	0.500760	—1.8434
204	0.9041	0.543497	0.3606	0.545027	0.541973	—1.1715
202	0.8898	0.566369	0.3234	0.568250	0.564497	0.2649
200	0.8763	0.554787	0.3215	0.556691	0.552892	1.3249
198	0.8594	0.501211	0.3582	0.502859	0.499571	2.6402
196	0.8415	0.415086	0.4264	0.416223	0.413952	3.2521
194	0.8254	0.315707	0.5097	0.316257	0.315159	3.3452
192	0.8130	0.220548	0.5925	0.220786	0.220311	2.9297
190	0.8051	0.140051	0.6651	0.140101	0.140002	2.5699

In order to obtain more complete absorption data a second experiment was run on mitochondria in which a shorter path length was chosen. In addition, a solubilized or molecularly dispersed state was sought in which the $[\theta]^{224}$ corresponded closely to the approximate value of $[\theta]^{224}_{Cl} = -1.6 \cdot 10^4$ noted above. Fitting the long wavelength absorption data of Curve b in Fig. 4 in the 240–300-nm wavelength range and using the indices of refraction given in Table I it is possible using Eqn. 11 to calculate A_S through the region of interest, *i.e.* 240–190 nm. These values are given in Table II. Subtracting the values of A_S from Curve b in Fig. 4 allowed calculation of A'_{susp} of Eqn. 3. If we now assume that a solubilized state with the same $[\theta]^{224}$ as our initial approximation, Eqn. 4, has an approximately correct absorption curve, we may use the absorption curve c of Fig. 4 as A_{soln}. Q_A is then calculated using Eqn. 2.

The expression used to calculate the distorted curve of poly-L-glutamic acid[15] was

$$[\theta]_{susp} = \frac{3300}{C_0 l}[Q_A(A_L - A_R) - (A_{SL}A_L - A_{SR}A_R) + (A_{SL} - A_{SR})] \quad (12)$$

By introducing the $[m]$ for an α-helical system with a $[\theta]^{224}_{Cl}$ of our initial approximation we can calculate $\Delta[\theta]_{DS}$ using Eqns. 5–10. Our correction at this stage is

$$[\theta]_{corr} \simeq \frac{[\theta]_{susp}}{Q_A - A_S} - \Delta[\theta]_{DS} \tag{13}$$

This result is given in Fig. 3 as Curve d. Realizing for solutions that

$$[\theta]_{corr} = \frac{3300(A_L - A_R)}{C_0 l} \tag{14}$$

we rewrite Eqn. 13 in the form of Eqn. 12, thus

$$[\theta]_{susp} = \frac{3300}{C_0 l}[Q_A(A_L - A_R) - A_S(A_L - A_R) + (A_{SL} - A_{SR})] \tag{15}$$

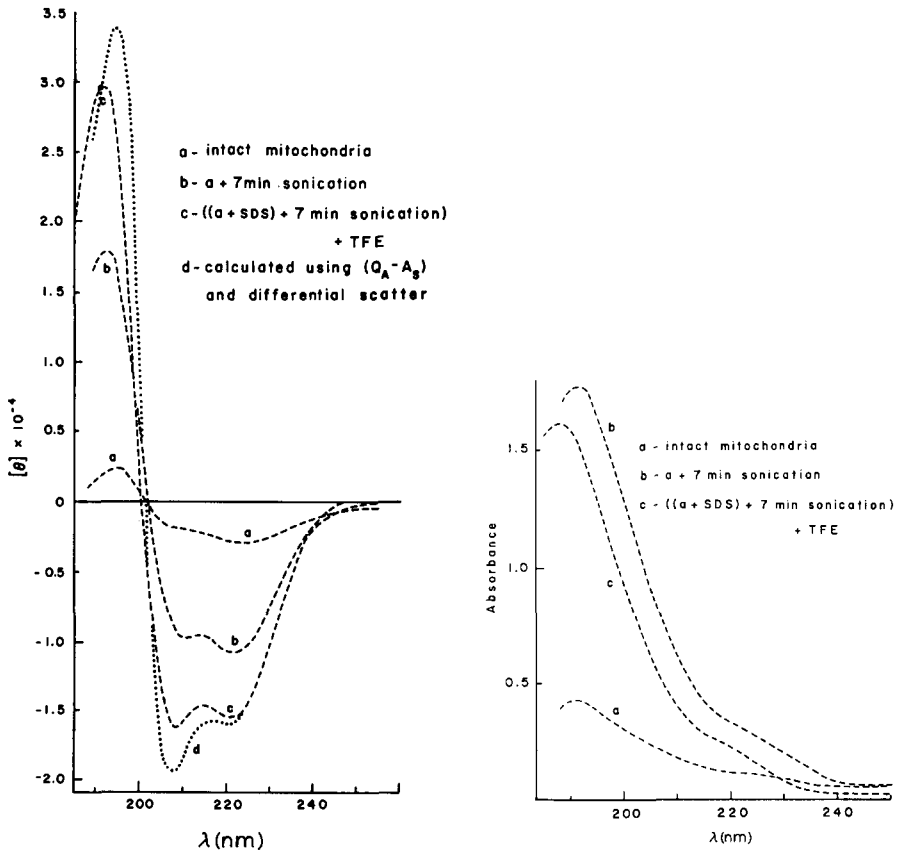

Fig. 3. Circular dichroism curves of mitochondria. Curve a is for the intact mitochondria and Curve b is the spectrum obtained after 7 min of sonication. The concentration of protein was 2.24 mg/ml and the path length used was 0.10 mm. Curve c is a solubilized state of the mitochondrial membrane in which the $[\theta]^{224}$ is closely that initially approximated for the corrected mitochondrial membrane (see text for discussion). The state in Curve c was obtained by addition of sodium dodecyl sulfate (SDS) followed by sonication and then addition of four parts of trifluoroethanol (TFE). Curve d is the calculated curve using the $Q_A - A_S$ correction and removal of the differential scatter effect, $\Delta[\theta]_{DS}$.

Fig. 4. Absorption curves obtained simultaneously with the circular dichroism curves in Fig. 3. With the shorter path length the absorption maximum could be obtained.

Comparing Eqns. 15 and 12 it is apparent that the second term is not the same. While this improvement could be achieved by an iterative procedure solving explicitly for successively better values of A_L and A_R it is sufficient to note that inclusion of the second term would bring Curve d in Fig. 3 closer to Curve c.

The result of recognizing the distortions and approximately correcting for them is that Curves c and d of Fig. 3 closely approximate the correct circular dichroism spectra for mitochondrial membranes. The fact that Curves c and d are so close suggests a simpler approach may be used to obtain complete spectra. This approach, called the pseudo reference state approach, will be demonstrated below for the red blood cell membranes.

Red blood cell membranes

The circular dichroism data on red blood cell membranes are given in Fig. 5. It is seen that sonication of previously frozen samples of membrane resulted in a large increase in ellipticity and in curves which are typical of α-helical systems. Fig. 6 contains the simultaneously recorded absorption spectra. As above, we proceed with an approximation of the ellipticity at 224 nm. Using the 80% trifluoroethanol solution as $A'_{susp} = 0.48$ and the absorption data of Fig. 6 $A_{susp} = 0.66$, from Eqn. 3 we have $A_S^{224} \simeq 0.18$ giving, from Eqn. 4, an initial approximation of

$$[\theta]_{C1}^{224} = \frac{-1.34 \cdot 10^4}{(1 - 0.18)} = -1.63 \cdot 10^4$$

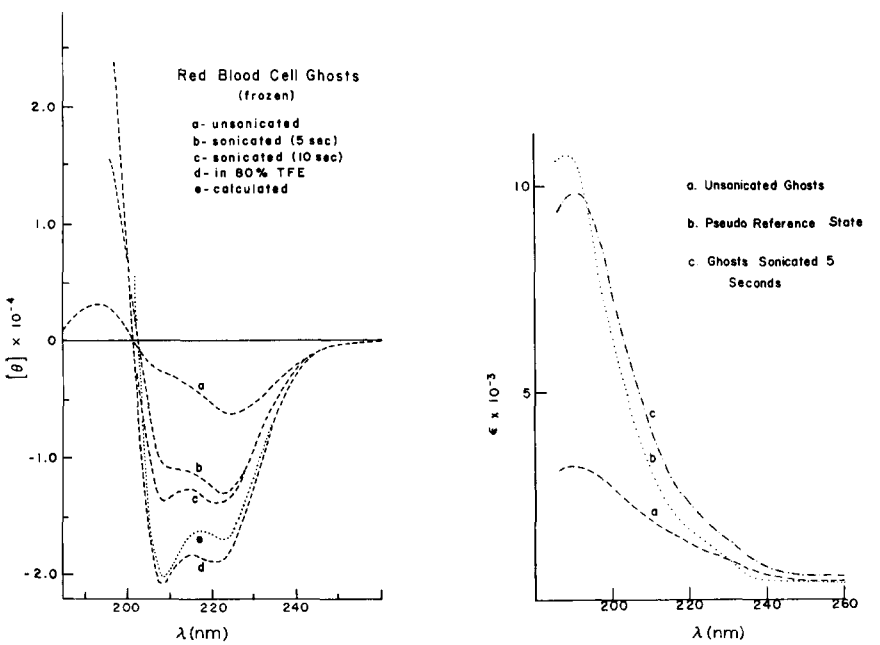

Fig. 5. Circular dichroism curves of red blood cell membranes.

Fig. 6. Absorption curves for red blood cell membranes. Curves a and c were obtained simultaneously with Curves a and c of Fig. 5.

The value at 224 nm can be improved, and a complete calculation of the corrected ellipticity curves can be obtained by more fully utilizing the solubilized state. It was seen in Fig. 3 that a solubilized state can be found which closely approximates the corrected values. In Fig. 5 the curve in 80% trifluoroethanol came closer to the approximated value at 224 nm. It should be noted that in the several ways that one can achieve the solubilized state the absorption at 224 nm is relatively constant, whereas the circular dichroism spectra can be greatly different. Thus, one can approximate $[\theta]_{Cl}^{224}$ and then search for the solvent system which most closely matches the calculated ellipticity value at 224 nm. Once an adequate curve is obtained it can be used as a pseudo reference state to further improve the value at 224 nm and to obtain a more complete curve.

Pseudo reference state approach

Since the general shape of the circular dichroism curves is that of α-helical systems, we will assume that the same relationship exists between absorption and circular dichroism in our membrane system as exists with the α-helix–random coil systems. Accordingly, we can calculate a fraction which is the difference between the ellipticity of the pseudo reference state, $[\theta]_{PR}^{224}$, and the initial approximation at 224 nm and divide it by the difference between the ellipticities of α-helical and disordered poly-L-glutamic acid at that wavelength, *i.e.* $-3.47 \cdot 10^4$ and $0.29 \cdot 10^4$, respectively,

$$\Delta f = \frac{[\theta]_{PR}^{224} - [\theta]_{Cl}^{224}}{-3.47 \cdot 10^4 - 0.29 \cdot 10^4} \tag{16}$$

On going from α-helix to random coil the extinction coefficient at 192 nm changes by approx. 3000. The change in absorbance at 192 nm which corresponds to the difference in ellipticity at 224 nm is

$$\Delta\varepsilon^{192} = \Delta f \cdot 3000 \tag{17}$$

and the change in absorption at 192 nm is

$$\Delta A^{192} = \Delta\varepsilon^{192}Cl \tag{18}$$

An initial absorption correction for a true reference state at 192 nm A_{Cl}^{192} would be

$$A_{Cl}^{192} = A_{PR}^{192} + \Delta A^{192} \tag{19}$$

Now the difference between α-helix and random-coil ellipticities at 192 nm for poly-L-glutamic acid is $8.8 \cdot 10^4$. This allows an initial approximation to the ellipticity at 192 nm, *i.e.*

$$[\theta]_{Cl}^{192} = [\theta]_{PR}^{192} - 8.8 \cdot 10^4 \Delta f \tag{20}$$

Combining Eqns. 2 and 3 for a first iteration

$$Q_{A1}^{192} = \frac{A_{susp}^{192} - A_{S1}^{192}}{A_{Cl}^{192}} \tag{21}$$

Rewriting Eqn. 1 we have

$$A_{S1}^{192} = Q_{A1}^{192} - \frac{[\theta]_{susp}^{192}}{[\theta]_{C1}^{192}} \tag{22}$$

Substituting Eqn. 22 into Eqn. 21 and solving for Q_{A1}^{192} we have

$$Q_{A1}^{192} = \frac{A_{susp}^{192} + \dfrac{[\theta]_{susp}^{192}}{[\theta]_{C1}^{192}}}{1 + A_{C1}^{192}} \tag{23}$$

Since A_{susp}^{192} and $[\theta]_{susp}^{192}$ are known experimentally, and $[\theta]_{C1}^{192}$ and A_{C1}^{192} can be calculated from Eqns. 19 and 20, we can calculate Q_{A1}^{192}. With a value for Q_{A}^{192} and the DUYSENS relationship to absorption along the diameter of the particle, A_P,

$$Q_{A1}^{192} = \frac{3}{2A_{P1}^{192}} \left\{ 1 - \frac{2\left[1 - (1 + A_{P1}^{192})e^{-A_{P1}^{192}}\right]}{(A_{P1}^{192})^2} \right\} \tag{24}$$

With A_{P1}^{192} calculated we can correct for absorption flattening at 224 nm, *i.e.*

$$A_{P1}^{224} = \frac{A_{P1}^{192} \cdot A_{PR}^{224}}{A_{C1}^{192}} \tag{25}$$

By Eqn. 24 we have Q_{A1}^{224} to give a corrected absorption due to scatter at 224 nm, *i.e.*

$$A_{S1}^{224} = A_{susp}^{224} - Q_{A1}^{224} \cdot A_{PR}^{224} \tag{26}$$

With a new A_{S1}^{224} and a Q_{A1}^{224} we can calculate an improved ellipticity at 224 nm that is $[\theta]_{C2}^{224}$ which can then be used in Eqn. 16 to start a second iteration. By Eqns. 24 and 25 this can be done at all wavelengths and the iterations continue until no more improvement is seen. The result for the red blood cell membranes is given as Curve e in Fig. 5.

The iterations improved the initial approximation, $[\theta]_{C1}^{224}$ from $-1.63 \cdot 10^4$ to $-1.70 \cdot 10^4$ and that at 192 nm from $3.1 \cdot 10^4$ to $3.4 \cdot 10^4$. This approach will be used on the plasma membranes and sarcotubular vesicles. It would appear that the initial approximation of $[\theta]_{C1}^{224}$ is quite close to the more extensive calculations. This suggests that simply finding a solvent system which gives a value at 224 nm which is close to $[\theta]_{C1}^{224}$ may be a useful procedure. It is interesting to note in this connection that different solvent systems are required, for example compare the pseudo reference states in Figs. 3 and 5. Accordingly, different structural aspects may be implied. Also it may be noted that differential scatter is greater for mitochondrial membranes than for red blood cell membranes.

REFERENCES

1 B. KE, *Arch. Biochem. Biophys.*, 112 (1965) 554.
2 B. KE, in L. P. VERNON AND G. R. SEELY, *The Chlorophylls*, Academic Press, New York, 1966, p. 427.
3 D. F. H. WALLACH AND P. H. ZAHLER, *Proc. Natl. Acad. Sci. U.S.*, 56 (1966) 1552.
4 J. LENARD AND S. J. SINGER, *Proc. Natl. Acad. Sci. U.S.*, 56 (1966) 1828.
5 D. W. URRY, M. MEDNIEKS AND E. BEJNAROWICZ, *Proc. Natl. Acad. Sci. U.S.*, 57 (1967) 1043.
6 W. F. H. M. MOMMAERTS, *Proc. Natl. Acad. Sci. U.S.*, 58 (1967) 2476.
7 D. F. H. WALLACH AND A. S. GORDON, in J. JARNEFELT, *Regulatory Function of Biological Membranes*, Elsevier, Amsterdam, 1968.
8 J. M. STEIM AND S. FLEISCHER, *Proc. Natl. Acad. Sci. U.S.*, 58 (1967) 1292.
9 J. LENARD AND S. J. SINGER, *Science*, 159 (1968) 739.
10 D. W. URRY AND T. H. JI, *Arch. Biochem. Biophys.*, 128 (1968) 802.
11 T. H. JI AND D. W. URRY, *Biochem. Biophys. Res. Commun.*, 34 (1969) 404.
12 A. S. SCHNEIDER, M. J. T. SCHNEIDER AND K. ROSENHECK, *Proc. Natl. Acad. Sci. U.S.*, 66 (1970) 793.
13 D. W. URRY, in D. W. URRY, *Spectroscopic Approaches to Biomolecular Conformation*, American Medical Association Press, Chicago, 1970, p. 33.
14 D. W. URRY, T. H. HINNERS AND L. MASOTTI, *Arch. Biochem. Biophys.*, 137 (1970) 214.
15 D. W. URRY AND J. R. KRIVACIC, *Proc. Natl. Acad. Sci. U.S.*, 65 (1970) 845.
16 L. N. M. DUYSENS, *Biochim. Biophys. Acta*, 19 (1956) 1.
17 J. R. KRIVACIC, D. E. WISNOSKY AND D. W. URRY, *Anal. Biochem.*, in the press.
18 D. W. URRY, L. MASOTTI AND J. R. KRIVACIC, *Biochem. Biophys. Res. Commun.*, 41 (1970) 521.
19 D. W. URRY, T. A. HINNERS AND J. KRIVACIC, *Anal. Biochem.*, 37 (1970) 85.
20 L. MASOTTI, D. W. URRY AND J. R. KRIVACIC, in preparation.
21 A. CRANE, J. L. GLENN AND D. E. GREEN, *Biochim. Biophys. Acta*, 22 (1956) 476.
22 T. T. DODGE, C. MITCHELL AND D. J. HANAHAN, *Arch. Biochem. Biophys.*, 100 (1963) 119.
23 J. R. KRIVACIC AND D. W. URRY, *Anal. Chem.*, 42 (1970) 596.
24 D. SINCLAIR AND V. K. LAMER, *Chem. Rev.*, 44 (1949) 245.
25 D. W. URRY, in J. O. HIRSCHFELDER AND D. HENDERSON, *Chemical Dynamics*, Wiley, New York, 1971, p. 581.
26 A. L. LEHNINGER, *The Mitochondrion*, Benjamin, New York, 1965, p. 206.
27 J. M. WRIGGLESWORTH AND L. PACKER, *Arch. Biochem. Biophys.*, 133 (1969) 194.